J Solid State Electrochem (2014) 18:1443–1456
DOI 10.1007/s10008-014-2427-x

ORIGINAL PAPER

Aqueous and nonaqueous lithium-air batteries enabled by water-stable lithium metal electrodes

Steven J. Visco · Vitaliy Y. Nimon · Alexei Petrov · Kirill Pridatko
Nikolay Goncharenko · Eugene Nimon · Lutgard De Jonghe
Yury M. Volfkovich · Daniil A. Bograchev

Received: 21 August 2013 / Revised: 3 February 2014 / Accepted: 10 February 2014 / Published online: 28 March 2014

Abstract The extremely high theoretical energy density of the lithium-oxygen couple makes it very attractive for next-generation battery development. However, there are a number of challenging technical hurdles that must be addressed for Li-Air batteries to become a commercial reality. In this article, we demonstrate how the invention of water-stable, solid electrolyte-protected lithium electrodes solves many of these issues and paves the way for the development of aqueous and nonaqueous Li-Air batteries with unprecedented energy densities. We also show data for fully packaged Li-Air cells that achieve more than 800 Wh/kg.

Keywords Lithium · Air · Battery · Solid electrolyte · LATP · Protected lithium electrode · PLE

Abbreviations

c_s	Concentration of species s
$c_{0,\mathrm{Lim},s}$	Solubility limit of species s in free electrolyte
$c_{\mathrm{Lim},s}$	Solubility limit of species s in a porous medium
D_s	Diffusion coefficient of species s
$D_{s,M}^{\mathrm{eff}}$	Effective diffusion coefficient of species s in porous medium M
F	Faraday's constant
$H(x)$	Heaviside step function
i_0	Exchange current density
$J_{\mathrm{dep},M}$	Kinetic rate constant of product precipitation in medium M
j^{Li}	Volumetric reaction current
k	Conductivity of free electrolyte
k_M^{eff}	Effective conductivity of electrolyte in porous medium M
k_A	Dissolution rate constant
K_M	Kinetic coefficient of precipitation
$n_{\mathrm{Li_2O_2}}$	Amount of discharge product formed during the previous cycles
r_{min}	Radius of the smallest pores filled with electrolyte
S	Specific surface density
t_+^0	Transference number for Li cations
t_{char}	Characteristic aging time
t_{c}	End of the previous discharge cycle
T	Temperature
V_s	Molar volume of species s
α	Transfer coefficient
α_M	Archie's exponent of medium M
γ_M	Difference between liquid electrolyte/pore wall and discharge product/pore wall interface energies in medium M
ε_M	Porosity of medium M
η	Overpotential of reaction
μ_s	Molar mass of species s
ρ_s	Density of species s
φ_e	Electrolyte potential

S. J. Visco · V. Y. Nimon (✉) · A. Petrov · K. Pridatko · N. Goncharenko · E. Nimon · L. De Jonghe
PolyPlus Battery Company, 2431 5th Street, Berkeley, CA 94710, USA
e-mail: vnimon@polyplus.com

Y. M. Volfkovich · D. A. Bograchev
Frumkin Institute of Physical Chemistry and Electrochemistry RAS, Moscow, Russia

Introduction

Galvanic couples based on the use of ambient oxygen offer significant gravimetric and volumetric advantages relative to conventional couples. Since the positive electrode (O_2) contributes no weight to the battery (prior to cell discharge), the theoretical energy density for metal-air couples, $M+xO_2=MO_{2x}$, can be exceptionally high. Metal-air battery chemistry development has been based almost exclusively on the use of

water-based electrolytes; certainly, all commercial zinc-air batteries use aqueous electrolyte. However, since Zn, Al, and Fe corrode rapidly at low pH, aqueous electrolytes for metal-air cells use concentrated KOH to limit self-discharge. Unfortunately, once conventional aqueous metal-air cells are activated and oxygen is allowed to enter the cathode, O_2 reacts directly with the zinc leading to relatively high self-discharge rates which limit the commercial markets available to Zn-Air batteries. Another major problem with metal-air batteries using alkaline electrolytes is the tendency to absorb CO_2 from ambient air which reacts with the KOH electrolyte to form poorly soluble K_2CO_3, a process known as carbonation, which degrades cell performance. Battery scientists have been aware of these problems for decades, but neither issue has been solved to date. The carbonation problem could be addressed by scrubbing CO_2 from the ambient air stream, but this is impractical for most battery applications. When one considers replacement of the zinc anode with a lithium anode, the problem of self-discharge appears to be so untenable that this galvanic couple would seem to be unworthy of serious consideration. Notably, due to the invention of the water-stable protected lithium electrode, it now appears that the Li-Air couple may be the only metal-air couple where self-discharge can be completely eliminated.

Although the exceptionally high theoretical energy density for the lithium-oxygen couple has attracted the attention of battery scientists for decades, reactivity of lithium metal with atmospheric moisture has precluded practical development of this intriguing technology. The invention of the protected lithium electrode (PLE) by PolyPlus Battery Company has enabled the development of a new generation of lithium battery technologies utilizing electrolytes that would normally react with lithium metal. These unique protected electrodes are enabling for high energy density lithium-air and lithium-water batteries [1–5]. PLEs utilize water-stable, high Li^+ conductivity solid electrolytes to chemically isolate a lithium core from the external environment (described below). In this way, lithium electrodes can be used in combination with aqueous and aggressive nonaqueous electrolytes, a practical necessity for both lithium-air and lithium-water batteries.

There are several types of lithium-air technology [6, 7] which can be broadly divided by the choice of electrolyte, either aqueous or nonaqueous (Table 1). Although the choice of nonaqueous electrolyte allows the use of bare lithium foil, it also introduces a number of complex problems including the extremely low solubility of the cell reaction product, Li_2O_2, as well as reactivity of peroxide with most commonly used lithium battery electrolytes. For the case of nonaqueous Li-Air, most researchers use anhydrous oxygen to avoid corrosion of the bare Li electrode by ambient moisture. The use of bare unprotected lithium greatly limits the choice of electrolytes (due to reaction with lithium) and precludes the use of air due to rapid corrosion of the Li metal electrode by moisture. Some groups have reported ex situ passivation of lithium by carbonate electrolytes [8] or the use of oxidizing additives [9] like $LiNO_3$ to form a protective solid electrolyte interface (SEI) allowing the use of aggressive solvents like amides and sulfoxides. Although it is unclear that this approach is fully protective or that the SEI will survive extended cycling, preliminary results are interesting. PolyPlus invented and patented water-stable PLEs [2, 4]. We described PLEs and lithium-air primary and rechargeable batteries based on them publicly for the first time in Nara, Japan [10–12]. The essential concept is to use a dense, pinhole-free Li^+ solid electrolyte to chemically isolate the lithium electrode (Li, Li_xC, Li_xSi, etc.) from the positive electrode (Fig. 1). The ceramic electrolyte most commonly used is based on the lithium analog of NASICON [13] with a composition of $Li_{1+x+y}(M, Al, Ga)_x \quad (Ge_{1-q}Ti_q)_{2-x}Si_yP_{3-y}O_{12}$ and typically is of the composition $Li_{1.3}Al_{0.3}Ti_{1.7}(PO_4)_3$ (LATP) produced in Japan by Ohara Corporation and in the USA by Corning. Although lithium analogs of NASICON are stable to water, they are not stable to lithium, requiring the incorporation of an interlayer which can be solid state (i.e., Li_3N), polymeric, ionic liquid, or nonaqueous liquid electrolyte. Some groups prefer to call this a "dual electrolyte" system, but it all dates back to original PLE concept and patents. This advance now appears to be critical to the practical development of both nonaqueous and aqueous lithium-air and lithium-sulfur batteries. The PLE also affords an elegant solution to the investigation and development of the air electrode for both aqueous and nonaqueous Li-Air chemistries.

Table 1 Lithium-air cell types

Electrolyte	Theoretical energy density (end of discharge)	Anode	Type	OCV
Nonaqueous $2\,Li + O_2 = Li_2O_2$	3,450 Wh/kg 8,000 Wh/l	Unprotected (bare Li)	Type A1	2.96 V
		Protected (PLE)	Type A2	
Aqueous $4\,Li + O_2 + 2\,H_2O =$ 4 LiOH (simplified)	3,850 Wh/kg 7,000 Wh/l	Unprotected (bare Li)	Not possible	3.45 V
		Protected (PLE)	Type B	

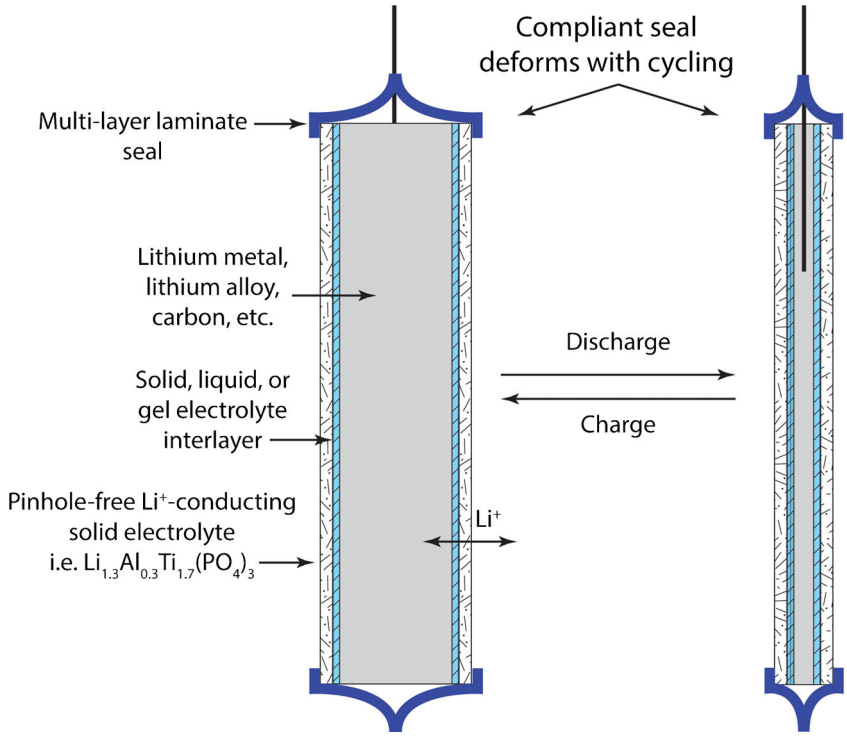

Fig. 1 Schematic of protected lithium electrode

In conventional aqueous metal-air cells, the products of the cell reaction are contained in the anode; in zinc-air cells, the zinc suspension is converted to ZnO as the cell reaction proceeds, whereas the structure and composition of the air electrode are essentially unchanged as the cell is discharged. This is fundamentally different in lithium-air technology since the lithium anode cannot accommodate the product of cell reaction. In a Li-Air cell, the air electrode must facilitate oxygen reduction and evolution as well as accommodate a substantial amount of reaction product while still functioning as an air electrode throughout cell discharge. The engineering of such a structure is certainly nontrivial. Among the key differences between the nonaqueous and aqueous air electrodes is that for aqueous systems, this electrode functions as a gas diffusion electrode with hydrophobic domains creating channels for O_2 gas transport, whereas in the nonaqueous case, the electrode is usually flooded. This fact highlights one of the key advantages of aqueous Li-Air over nonaqueous: the existence of three-phase boundaries throughout the aqueous air electrode leads to much faster oxygen transport and better electrode kinetics and therefore much higher sustained current densities. Another issue for the nonaqueous chemistry is solvent loss from the air electrode which would be unavoidable in an open system. Accordingly, any practical nonaqueous Li-Air battery would almost certainly need to be based on a closed system running on anhydrous oxygen, and such constraints may override the energy density advantages that Li-Air chemistry offers. Herein, we discuss some of the critical hurdles in lithium-air chemistry and our own progress in both aqueous and nonaqueous Li-Air systems.

PolyPlus has studied both the nonaqueous and aqueous Li-Air chemistries in some detail to determine baseline performances for both approaches and to initiate commercialization of ultra lightweight rechargeable batteries. Assuming the use of commercially available components and reasonable values for components still in development, one can project Li-Air cell energy densities of about 1,000 Wh/l and 600 Wh/kg for a reversible electrode capacity of 5 mAh/cm^2, implying that Li-Air cells should sustain current densities of at least 1 mA/cm^2 (C/5) in order to realize broad commercial application.

In the mid-2000s, interest in Li-Air batteries rose tremendously as a number of research groups claimed to be on the path to batteries with an order of magnitude improved energy density, motivated by the extremely high energy density of the Li/O_2 couple. If one does not include the weight of the oxygen consumed as the discharge reaction progresses, the specific energy for the Li/O_2 couple is 11,600 Wh/kg. Although metal-air batteries gain weight as the cell reaction progress and O_2 is converted to lithium peroxide (yielding a theoretical maximum of 3,450 Wh/kg), the average specific energy over the course of cell discharge is well over 7,000 Wh/kg, approaching that of gasoline and providing ample motivation for cell developers.

The earliest work in nonaqueous Li-Air chemistry was reported by Abraham [14]. These studies were done with bare unprotected lithium, dry oxygen, and polymer electrolytes plasticized by organic carbonates. In fact, most early studies of nonaqueous Li-Air batteries relied heavily on the use of electrolytes based on organic carbonate solvents typically used in Li-ion batteries.

However, an early paper by Aurbach and Yeager [15] pointed out that carbonate electrolytes are unstable to nucleophilic attack by superoxide anion radical (O_2^-), an intermediate in the reduction of oxygen. Consequently, early results that demonstrated extended cycling of Li-O_2 batteries and improvements due to electrocatalysts were greatly affected by solvent degradation and oxidation of those degradation products. Since that time, a number of groups have conducted careful investigations of those degradation phenomena [16, 17], followed by a search for stable nonaqueous electrolytes for Li-O_2 batteries [18].

In 2005, PolyPlus Battery Company expanded the exploration of a number of nonaqueous Li-Air chemistries based on the use of PLEs in combination with solvents known to be stable to peroxide (and superoxide) but not necessarily to lithium metal including amides, sulfoxides, and nitriles [19]. A schematic drawing of nonaqueous Li-Air cells having a PLE is shown in Fig. 2a. Although the theoretical energy densities for Li-Air chemistries are certainly large (Table 1), practical cell performance will not exceed that of commercial Li-ion batteries until Li-Air cells reach certain threshold current densities and capacities. However, nonaqueous Li-Air performance is typically limited to very low current densities, often below 0.1 mA/cm^2, and cycled capacity is typically less than 1.0 to 1.5 mAh/cm^2. Another concern for nonaqueous Li-Air technology is the irreversible and rapid reaction of lithium peroxide with carbon dioxide [Li_2O_2 (s)+CO_2=Li_2CO_3 (s)+1/2 O_2]. In fact, the NASA space program proposed the use of Li_2O_2 to scavenge CO_2 in manned spaceflight operations [20].

The first examples of aqueous Li-Air batteries were reported by PolyPlus Battery Company [2, 10–12] enabled by the invention of the protected lithium electrode. One of the commonly recognized problems with aqueous metal-air chemistries is the high rate of self-discharge due to direct reaction of oxygen with the negative electrode. In stark contrast, the self-discharge rate of our aqueous Li-Air cell is effectively zero, due to the presence of a solid electrolyte membrane which chemically isolates the metal electrode from the positive electrode compartment (Fig. 2b). The use of a Li^+-conductive solid electrolyte in aqueous electrolyte also begs the question of stability of the ceramic LATP as a function of pH (addressed below). As can be seen from the following, the performance of aqueous Li-Air cell technology, both primary and secondary, is quite promising.

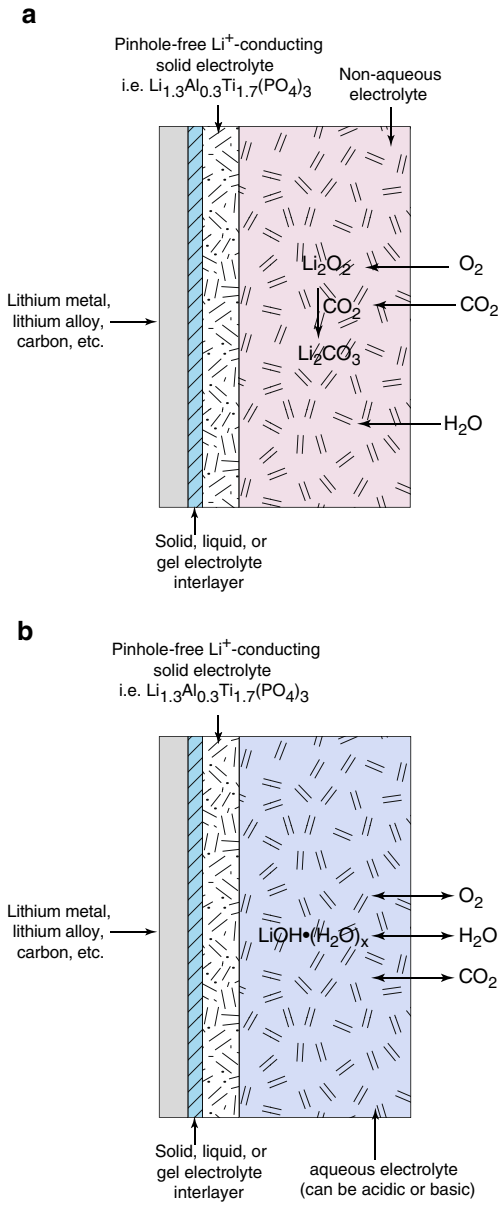

Fig. 2 Schematics of Li-Air cells employing PLE. **a** With nonaqueous electrolyte. **b** With aqueous electrolyte

Experimental

All operations for the preparation of nonaqueous electrolytes were performed in an MBraun glove box filled with Ar gas. Moisture and oxygen concentrations inside the glove box did not exceed 0.5 ppm. Solvents used for preparation of nonaqueous electrolytes, including dimethyl formamide (DMF), diglyme (DG), tetraglyme (TG), ethyl acetate (EA), and sulfolane, were obtained from Aldrich Chemicals and dried with 4 Å molecular sieves. Tris(pentafluorophenyl)borane (TPFB) obtained from Aldrich Chemicals was used as received. Electrolyte salts including lithium bis(trifluoromethylsulfonyl)imide (LiTFSI), and $LiBF_4$, were dried under vacuum at 120 °C for several days prior to electrolyte preparation. The moisture content in prepared nonaqueous electrolytes did not exceed 10 ppm except electrolytes containing TPFB, in which the moisture content was close to 60 ppm.

Li_2O_2 (99.9 % purity) was obtained from Pfaltz & Bauer Inc. Li_2O_2 was placed into two vials—the first one containing DMF and the second one containing 0.25 M TPFB in DMF. Both mixtures were stirred for 1 week, and undissolved solids were allowed to settle down. The clear fractions of the mixtures were

removed with a syringe and then filtered using a Puradisc 25 Syringe Filter, 0.2 μm, obtained from GE Healthcare Life Sciences. The filtrates were sent to Maxxam Analytics (Canada) for lithium analysis. All chemicals used for preparation of aqueous electrolytes including LiCl, NH_4Cl, $LiNO_3$, NH_4NO_3, LiOH, malonic acid, citric acid, and imidazole were obtained from Aldrich Chemicals and used as received. H_3PO_4 and Na_2HPO_4 used for preparation of buffer solutions were also obtained from Aldrich Chemicals.

PLEs for rechargeable batteries utilized lithium metal foil with a thickness of 120 μm purchased from FMC Lithium. $Li_{1+x+y}(M, Al, Ga)_x(Ge_{1-q}Ti_q)_{2-x}Si_yP_{3-y}O_{12}$ ceramic membranes (single ion, Li^+, conductors) with conductivities in the range of 1.0 to 2.5×10^{-4} S/cm were obtained from Ohara Corporation in Japan and Corning Incorporated in the USA. Fully engineered high energy density primary Li-Air cells were based on double-sided PLEs as illustrated above and utilized ceramic membranes with a size of 50 mm×50 mm. We designed single-sided test cells for electrochemical testing of electrolytes and electrode materials for secondary Li-Air batteries with nonaqueous and aqueous electrolytes. PLEs were assembled as described previously [19]. Stability of the solid electrolyte membranes in aqueous electrolytes was measured in situ by monitoring the impedance evolution over time.

Cells for impedance measurements employed an LATP membrane having an RF sputtered gold film with a thickness of 300–400 nm on one side and aqueous electrolyte on the other side. The surface area of gold electrodes used for impedance measurements was 1.3 cm^2. A platinized platinum electrode served as a counter electrode (the impedance of the counter electrode did not contribute to the cell impedance due to the electrode's high surface area). The schematic of this cell is shown in Fig. 3a (insert). For comparison, we also obtained impedance spectra of an LATP membrane having sputtered gold films on both sides (Fig. 3b (insert)). The Li-Air test cells shown in Fig. 4 were built with a PLE utilizing 25.4 mm×25.4 mm ceramic membranes, a porous air cathode and a zirconia separator from Zircar Zirconia Inc. (USA). The air cathodes for all Li-Air cell configurations were prepared from an active mass containing Ketjenblack EC-600JD carbon black, polytetrafluoroethylene (PTFE) dispersion, and a catalyst based on manganese oxide. Li-Air cells with nonaqueous electrolytes were tested in an atmosphere of dry oxygen. Li-Air cells with aqueous electrolytes were tested in air with controlled humidity. Experimental results related to testing of Li-Air cells with aqueous electrolytes were obtained at 50 % relative humidity and 25 °C. Constant temperature and humidity levels were maintained using CSZ's Z-Plus test chambers (Cincinnati Sub Zero Industrial). Electrochemical impedance measurements were performed in the frequency range from 10 Hz to 1.0 MHz using a Solartron 1287 Electrochemical Interface and Solartron 1260 Impedance/gain-phase analyzer. A VMP-3 potentiostat/galvanostat from Bio-Logic (France) was used for linear sweep voltammetry experiments. Electrochemical

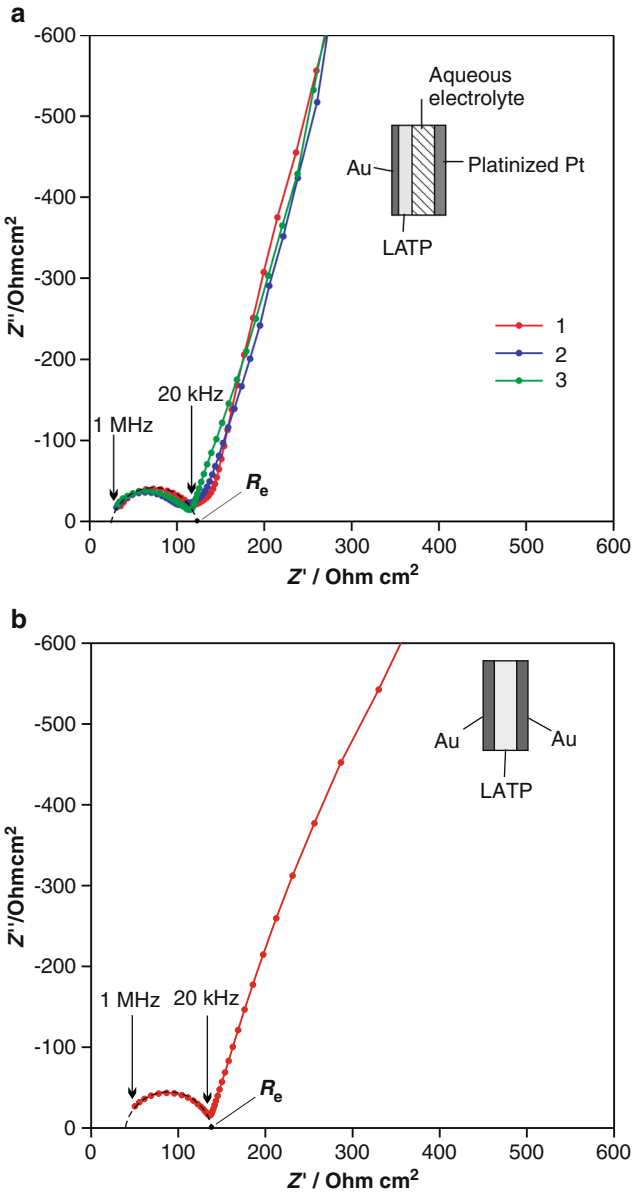

Fig. 3 **a** Impedance spectra for LATP membrane immersed in aqueous 4.0 M NH_4Cl+2.0 M LiCl electrolyte; *1*—no storage, *2*—57 days of storage, *3*—632 days of storage. Membrane thickness is 125 μm. *Insert* shows the schematic of the impedance cell. *Arrows* indicate characteristic frequencies. **b** Impedance spectra for LATP membrane sandwiched between two gold electrodes. Membrane thickness is 152 μm. *Insert* shows the schematic of the impedance cell. *Arrows* indicate characteristic frequencies

discharge/charge testing of Li-Air cells was performed using a Maccor 4000 battery tester.

Concentrations of Li_2O_2 dissolved in nonaqueous electrolytes based on DMF were measured by inductively coupled plasma optical emission spectrometry at Maxxam Analytics. The lithium analysis was carried out using a PerkinElmer Optima 2000 DV spectrometer. Relative error in lithium concentration determination did not exceed 10 %. Obtained lithium concentrations were recalculated into concentrations of Li_2O_2.

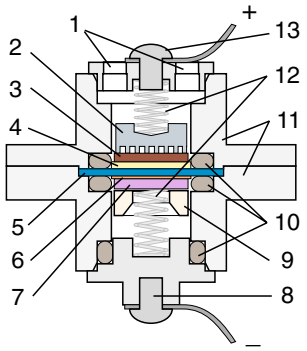

Fig. 4 Schematic of Li-Air test cell. *1*—air access holes, *2*—cathode current collector, *3*—air cathode, *4*—separator/electrolyte reservoir, *5*—solid electrolyte membrane, *6*—interlayer, *7*—lithium foil, *8*—anode terminal, *9*—anode holder, *10*—O-ring seals, *11*—plastic flanges, *12*—compression springs, *13*—cathode terminal

During discharge of primary Li-Air cells with aqueous electrolyte, ammonia levels in test chambers were monitored with a NOVA-SensorElite Ammonia Gas Detector obtained from Aztec Signal. The pH values of aqueous electrolyte after partial and full discharge of primary Li-Air cells were determined with BDH pH test strips from VWR.

Results and discussion

Nonaqueous Li-Air cells We studied the cycling behavior of Li-Air cells with electrolytes based on DMF. Bare lithium rapidly reacts with DMF; therefore, our Li-Air cells employed PLEs with LATP membranes. Electrochemical oxygen reduction in electrolytes based on DMF and tetraalkylammonium salts has been the subject of extensive research [21–23], and DMF was expected to be stable towards the products of oxygen reduction in Li-Air cells. Recently reported theoretical calculations of solvent reactivity [24] also confirm high stability of DMF against nucleophilic attack by superoxide.

One of the key problems with nonaqueous Li-O_2 chemistry is the extremely low solubility of the discharge product, Li_2O_2. We explored increasing the solubility of Li_2O_2 in DMF by the addition of anion receptors to the nonaqueous electrolyte in an attempt to improve the performance of the air electrode. The use of anion receptors for enhancement of Li_2O_2 dissolution and improvement of electrolyte conductivity has been discussed in literature [25–27]. However, since anion receptors are incompatible with bare lithium metal, to the best of our knowledge, the effect of anion receptors on Li-Air cell performance has never been actually tested. We performed such tests using Li-Air cells employing PLEs.

We had limited success with a commercially available anion receptor TPFB. Using ICP-OES analysis, it was found that Li_2O_2 solubility in DMF did not exceed 0.2 mmol/L, while in the presence of 0.25 M TPFB, it was close to 17 mmol/L. This increase in solubility resulted in improved cyclability. As shown in Fig. 5a, we obtained several charge–discharge cycles in Li-O_2 cells having a DMF-based electrolyte containing 0.25 M TPFB. However, even in the presence of TPFB, capacity fade during cycling was observed. If after the first discharge the cell was stored under open circuit conditions, the capacity fade was even more pronounced (Fig. 5b).

Here, we propose that solid discharge product aging significantly contributes to the observed capacity fade during cycling. Although the morphology of Li_2O_2 particles formed during discharge of Li-Air cells with nonaqueous electrolyte has been studied [28, 29] (see review in [30]), to the best of our knowledge, the effect of Li_2O_2 precipitate aging has not been described in the literature. We modified the mathematical model presented in [31] to describe this effect. It was assumed that at the low charge current densities used in our experiments, the oxygen released during charge dissolved into the electrolyte and did not contribute to gas porosity.

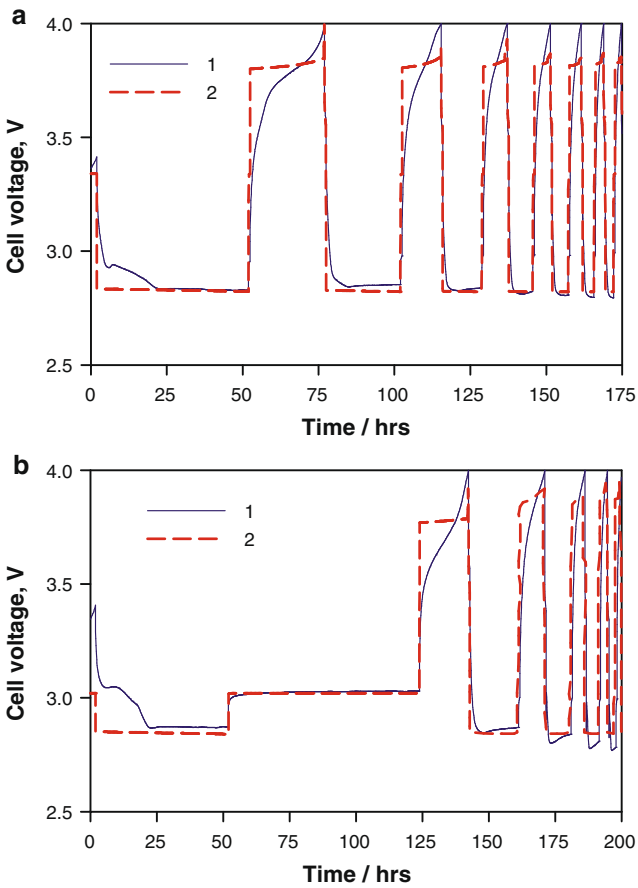

Fig. 5 Comparison of experimental (*1*) and calculated (*2*) cycling curves for Li-Air cells. Electrolyte: 0.5 M LiTFSI, 0.25 M TPFB in DMF. Discharge/charge rate was 0.1 mA/cm^2. Charge cutoff voltage was 4.0 V. **a** The first discharge lasted 50 h; capacities of the second and the following discharges were equal to those of the charges immediately preceding them. **b** The first discharge lasted 50 h and was followed by 72 h of rest at open circuit; capacities of the second and the following discharges were equal to those of the charges immediately preceding them

The model [31] was based on our experimental porosimetry data, which indicated that precipitation of the discharge product started in the small cathode pores (mesopores with radii less than 10 nm). The equations describing mass and charge transport, reaction current, mass balance, and discharge product precipitation and dissolution are presented in Table 2. The modified model introduces the phenomenon of discharge product aging which manifests itself as a decrease in precipitate dissolution rate.

In this system, the aging process is unique since it happens within small mesopores, where it is influenced by interaction with pore walls. We have demonstrated that the order of discharge product deposition in the pores of different sizes depends on the surface properties of the carbon pore wall–discharge product–liquid electrolyte system [31]. The discharge product aging also depends on the properties of this three-component system. In the literature, there are no theoretical models applicable to discharge product aging in such a complex system.

Equation (7) in Table 2 is the modified equation describing the rate of precipitation and dissolution of the discharge product. We assume that the rate of aging can be described with an exponential Eq. (8), where t_{char} is the characteristic aging time, t_c is the end of the previous discharge cycle, $n_{Li_2O_2}$ is the amount of discharge product formed during the previous cycles, and k_A is the dissolution rate constant.

Comparison of calculated and experimental cycling curves, both with and without rest (Fig. 5a, b), indicates that they are in satisfactory agreement. The experimental curves exhibit a gradual increase in voltage during charging; however, the calculated curves have a voltage plateau followed by a rapid increase in voltage.

The characteristic shape of the calculated curves is explained by the fact that in the model, the primary effect limiting the reaction is the decrease in concentration of dissolved Li_2O_2, resulting in a rapid rise in cathode overpotential to the 4-V limit, which corresponds to the end of charge. The gradual voltage increase observed in the experimental curves during charge is possibly related to side reactions resulting in the formation of lithium carbonate layer on the carbon air cathode surface [32].

The model predicts that at the end of each discharge, the volumetric fraction of solid discharge product increases from zero on the anode side of the electrolyte reservoir (separator) to a maximum at the cathode-air interface. This maximum volumetric fraction value increases with each charge–discharge cycle.

Values of the characteristic time for precipitate aging during each cycle were determined from the experimental cycling curves and are shown in Fig. 6. When the cycling procedure did not include a prolonged rest at open circuit, the characteristic time decreased rapidly with cycling until reaching its minimum value by the fourth cycle (Fig. 6a). For the cycling procedure with a 72-h rest after the first cycle, the minimum value was already reached by the second cycle (Fig. 6b).

The aging phenomenon can be explained by thermodynamically favorable coarsening of the solid discharge product (Li_2O_2), which leads to a decrease in the precipitate's effective surface area and dissolution rate constant. Aging occurs both during cell rest and charge. Experimentally, the aging effect

Table 2 Summary of model equations

Description	Model equation
Effective diffusion coefficient for species s in medium M	$D_{M,s}^{\text{eff}} = D_s \varepsilon^{\alpha_M}$ (1)
Effective diffusion equation for Li cations in medium M	$\frac{\partial \varepsilon c_{\text{Li}}}{\partial t} = \frac{\partial}{\partial x}\left(D_{M,\text{Li}}^{\text{eff}} \frac{\partial c_{\text{Li}}}{\partial x}\right) - \frac{1-t_+^0}{F} j^{\text{Li}}$ (2)
Effective diffusion equation for O_2 in medium M	$\frac{\partial \varepsilon c_{O_2}}{\partial t} = \frac{\partial}{\partial x}\left(D_{M,O_2}^{\text{eff}} \frac{\partial c_{O_2}}{\partial x}\right) - \frac{j^{\text{Li}}}{2F}$ (3)
Effective diffusion equation for Li_2O_2 in medium M	$\frac{\partial \varepsilon c_{Li_2O_2}}{\partial t} = \frac{\partial}{\partial x}\left(D_{M,Li_2O_2}^{\text{eff}} \frac{\partial c_{Li_2O_2}}{\partial x}\right) + \frac{j^{\text{Li}}}{2F} - J_{\text{dep},M}$ (4)
Effective conductivity for medium M	$k_M^{\text{eff}} = k\varepsilon^{\alpha_M}$ (5)
Charge transport equation for medium M	$\frac{\partial}{\partial x}\left(k_M^{\text{eff}} \frac{\partial \varphi_e}{\partial x}\right) + j^{\text{Li}} = 0$ (6)
Rate of Li_2O_2 precipitation and dissolution	
$J_{\text{dep}} = K_M\left(H\left(c_{Li_2O_2} - c_{\text{Lim},Li_2O_2}\right) - \theta H\left(c_{\text{Lim},Li_2O_2} - c_{Li_2O_2}\right)\right) \times \left(\frac{c_{Li_2O_2}}{c_{0,\text{Lim},Li_2O_2}} - \frac{c_{\text{Lim},Li_2O_2}}{c_{0,\text{Lim},Li_2O_2}}\right)^2$ (7)	
Ratio of kinetic coefficients of dissolution and precipitation	$\theta = n_{Li_2O_2} k_A \exp\left(-\frac{t-t_c}{t_{\text{char}}}\right)$ (8)
Kelvin equation	$\ln\left(\frac{c_{\text{Lim},Li_2O_2}}{c_{0,\text{Lim},Li_2O_2}}\right) = \frac{2\gamma_M V_{Li_2O_2}}{r_{\min} RT}$ (9)
Reaction current, Buttler-Volmer kinetics	$j^{\text{Li}} = Si_0\left(\frac{c_{O_2}}{c_{0,O_2}} \exp\left(\frac{\alpha\eta F}{RT}\right) - \frac{c_{Li_2O_2}}{c_{0,Li_2O_2}} \exp\left(-\frac{(1-\alpha)\eta F}{RT}\right)\right)$ (10)
Local mass balance	$\frac{\partial \varepsilon}{\partial t} = -\frac{\mu_{Li_2O_2}}{\rho_{Li_2O_2}} J_{\text{dep},M}$ (11)

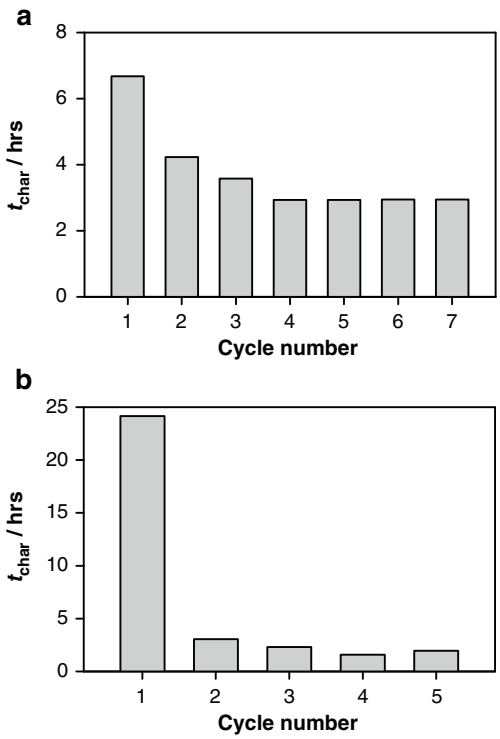

Fig. 6 Dependence of characteristic aging time on cycle number. **a** Testing procedure did not include a prolonged rest at open circuit. **b** Testing procedure included a 72-h rest at open circuit after the first discharge

leads to a decrease of dissolved lithium peroxide during charging and a corresponding rise in air cathode polarization. It is possible that the aging phenomenon is even more complex and involves additional processes, such as formation of thin-resistive lithium carbonate layer on the carbon air cathode surface. Lithium carbonate could be produced via reaction of the precipitate with CO_2 formed due to electrochemical oxidation of the solvent at high positive potentials or electrochemical oxidation of carbon air cathode surface [32].

In addition to studies of Li-Air cells having DMF electrolytes, we performed testing of lithium-air cells with glyme-based electrolytes (diglyme and tetraglyme), as well as with electrolytes based on sulfolane.

Diglyme and tetraglyme were chosen due to their lower volatility compared to DME (monoglyme). Importantly, glymes are not sufficiently stable in contact with lithium metal, especially during cycling, which is why in all known battery systems, DME is used in combination with another co-solvent, such as dioxolane or an organic carbonate, which forms a stable SEI. Cycling performance of Li-Air cells with glyme electrolytes can be correctly evaluated only if a PLE is employed. Sulfolane (in combination with EA co-solvent and $LiBF_4$ salt) was chosen because of its exceptional oxidative stability [33].

Cycling of nonaqueous lithium-air cells with glyme-based electrolytes is shown in Figs. 7 and 8. The cells exhibited a reversible capacity of slightly more than 1 mAh/cm^2 at a

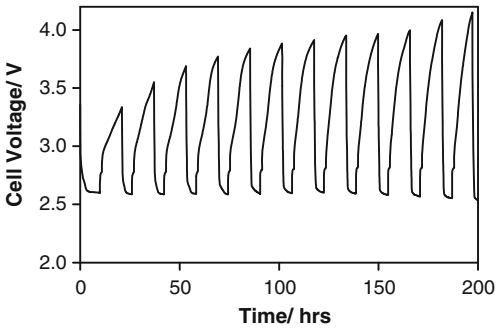

Fig. 7 Cycling performance of Li-Air cells. Electrolyte: 0.5 M LiTFSI in DG. Discharge rate was 0.25 mA/cm^2. Charge rate was 0.125 mA/cm^2. The first discharge lasted 10 h. The first charge capacity was 50 % of the first discharge capacity. Capacities of the second and the following discharges were equal to the capacities of the charges immediately preceding them or were limited by a cutoff voltage of 2.4 V. Capacities of the second and the following charges were equal to the capacities of the discharges immediately preceding them or were limited by a cutoff voltage of 4.15 V

discharge current density of 0.25 mA/cm^2. Although preliminary results with sulfolane (Fig. 9) are also interesting, we observed increasing polarization on charge and limited capacity on cycling. In order to achieve high specific energy and reasonable power density in an engineered battery, the lithium-air cells based on diglyme catholytes would require a fourfold improvement in reversible capacity at four times the current density shown here. Recently, several other groups have reported encouraging cycling of the O_2 electrode in nonaqueous electrolytes based on organic solvents such as sulfoxides [8, 34] and amides [9]; neither of which is stable to bare metallic lithium metal. Assuming that developers are successful in identifying nonaqueous electrolytes that permit reversible cycling of oxygen electrode, it appears likely practical cells will require a fully protected lithium electrode (an absolute for aqueous Li-Air). Still, even with the incorporation of a PLE, there are unresolved technical issues for nonaqueous lithium air including (1) evaporation of nonaqueous solvent

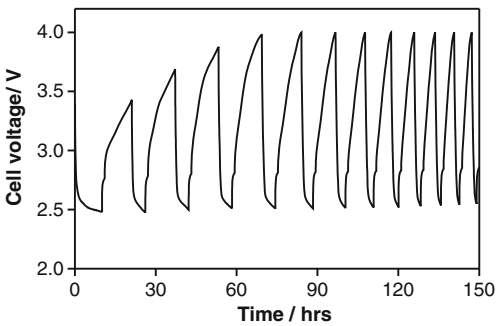

Fig. 8 Cycling performance of Li-Air cells. Electrolyte: 0.5 M LiTFSI in TG. Discharge rate was 0.25 mA/cm^2. Charge rate was 0.125 mA/cm^2. The first discharge lasted 10 h. The first charge capacity was 50 % of the first discharge capacity. Capacities of the second and the following discharges were equal to the capacities of the charges immediately preceding them or were limited by a cutoff voltage of 2.4 V. Capacities of the second and the following charges were equal to the capacities of the discharges immediately preceding them or were limited by a cutoff voltage of 4.0 V

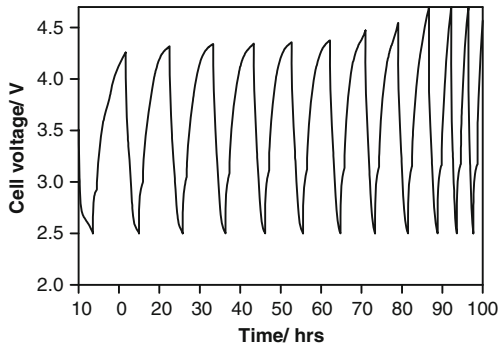

Fig. 9 Cycling performance of Li-Air cells. Electrolyte: 0.5 M $LiBF_4$ in sulfolane and EA mixture (1 to 1 by volume). Discharge rate was 0.25 mA/cm^2. Charge rate was 0.125 mA/cm^2. All discharge capacities were limited by a cutoff voltage of 2.5 V. All charge capacities were equal to the capacities of the discharges immediately preceding them or were limited by a cutoff voltage of 4.7 V

from the air electrode to the external environment; (2) uptake of water by the nonaqueous electrolyte; (3) irreversible reaction of Li_2O_2 with CO_2 leading to the formation of Li_2CO_3 and loss of electrode capacity; (4) flooding of the air electrode with nonaqueous electrolyte leading to slow oxygen transport; and (5) precipitation of insoluble Li_2O_2 in the pores of the air electrode leading to pore clogging and polarization of the air electrode. Some of the technical issues for nonaqueous Li-Air could be addressed with a closed system (no solvent loss) and anhydrous oxygen (no water or CO_2 contamination), although this approach would certainly degrade the system energy density. Assuming successful identification of a nonaqueous electrolyte stable to products of O_2 reduction and the use of a closed system with dry oxygen, there still remains the issue of poor solubility of Li_2O_2, flooding of the air electrode leading to poor electrode kinetics, and clogging of the porous oxygen electrode structure as cell discharge proceeds. In light of the above discussion, the list of promising electrolyte solvents for nonaqueous Li-Air batteries is relatively short at this time including amides, sulfoxides, and glymes, as described in a PolyPlus patent application in early 2006 [19]. To date, none of these electrolytes demonstrate the rate capability, cycling capacity (mAh/cm^2), or cycle life required for practical application.

Aqueous Li-Air cells Determination of stability of the ceramic membrane in aqueous electrolyte is not trivial and is certainly not measured properly by immersing the membrane into a large volume of concentrated acid or base. PolyPlus has determined the stability of the LATP ceramic membrane in a variety of aqueous electrolytes by in situ impedance spectroscopy using a volume of electrolyte corresponding closely to that used in a practical cell. There is no doubt that LATP membranes degrade in strong inorganic acid or base, particularly when there is a large excess of aqueous electrolyte, but this has little to do with realistic cell conditions. We have found that LATP membranes exhibit satisfactory stability, depending critically on the composition of the electrolyte, pH, and nature and concentration of the supporting salts. Our primary Li-Air cells utilize electrolytes based on NH_4Cl/LiCl and NH_4NO_3/$LiNO_3$. These electrolyte blends have the advantage of generating hygroscopic LiCl or $LiNO_3$ on cell discharge which scavenges H_2O from the external environment, alleviating the need to carry a stoichiometric quantity of water for the cell reaction. Since these electrolytes are slightly acidic prior to cell discharge, there is no uptake of CO_2 on exposure to ambient atmosphere. For rechargeable Li-Air cells, PolyPlus developed polyprotic organic acid-based electrolytes. Some of these polyprotic acids were found to degrade the performance of the LATP membranes as evidenced by a significant increase in the impedance arc corresponding to the total resistance of the membrane. Fortunately, we identified several polyprotic acid electrolytes in which LATP membranes exhibited excellent stability over time.

Primary aqueous Li-Air Lithium-air batteries share some common features with primary Zn-Air batteries including the use of a gas diffusion electrode for oxygen reduction. As discussed above, in a Li-Air battery, the products of cell discharge are stored in the air electrode which means that the cathode compartment must accommodate a large volume of solid reaction product. Our air electrode design can accommodate a tremendous amount of solid discharge product as demonstrated by the data shown in Fig. 10. We have designed and fabricated Li-Air cells with PLEs of approximately 10 Ah based on 50 mm × 50 mm solid electrolyte membranes and thick lithium foils (total thickness of approximately 2.5 mm). In these cells, the lithium capacity is matched with two air electrodes (filled with 6.8 ml of aqueous electrolyte each) and exposed to air. At a current density of 0.5 mA/cm^2, these air electrodes deliver an area-specific capacity of approximately 200 mAh/cm^2 (for a total capacity of 8,500 mAh) at an energy density of more than 600 Wh/kg for fully engineered cells. The cells tested at a current density of 0.3 mA/cm^2 delivered a

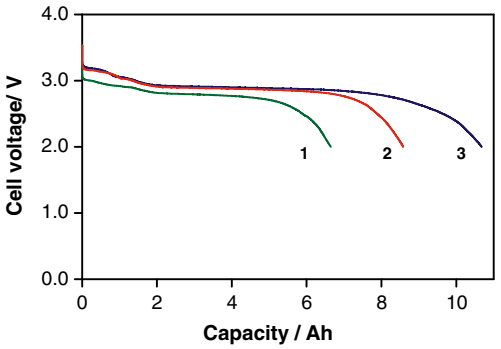

Fig. 10 Discharge of fully engineered primary Li-Air cells with aqueous electrolyte comprising 2 M LiCl and 4 M NH_4Cl. Discharge rate: *1*—1.0 mA/cm^2, *2*—0.5 mA/cm^2, *3*—0.3 mA/cm^2

massive specific energy of 800 Wh/kg; to the best of our knowledge, this is the highest specific energy ever reported for an electrochemical device (other than PolyPlus Li-water battery).

LATP membranes demonstrated excellent stability in NH_4Cl/LiCl and NH_4NO_3/$LiNO_3$ electrolytes employed in primary Li-Air cells. In Fig. 3a, we present the impedance spectra of an LATP membrane immersed in NH_4Cl/LiCl aqueous electrolyte after various periods of storage. In order to interpret the shape of impedance diagram in Fig. 3a, we also obtained impedance spectra for a LATP membrane sandwiched between sputtered gold electrodes (Fig. 3b). Similar impedance diagrams for LATP membranes having an ionically blocking inert electrode on each side have been previously reported by other groups and are widely used to determine the ionic conductivity of LATP membranes [35–37]. Equivalent circuits proposed in the literature for impedance of solid-state cells employing LATP membranes can be quite complex and usually include at least one constant phase impedance element [38, 39]. The low-frequency intercept with the *x* axis corresponds to the total active resistance of the LATP membrane R_e, which includes resistances of both grain boundaries and grains of polycrystalline LATP membranes. In our case, the ionic conductivity calculated from the value of R_e is 1.1×10^{-4} S/cm. Since LATP membranes in commercial Li-Air cells may be exposed to NH_4Cl/LiCl aqueous electrolyte for extended periods of time during storage, we determined the evolution of the impedance response over time. As seen in Fig. 3a, b, the impedance diagrams for the cell, where the ceramic LATP membrane is immersed in liquid electrolyte and the cell where the membrane is sandwiched between two gold electrodes, are almost identical, and the shape of the impedance plot in Fig. 3a exhibits negligible changes during storage of up to 21 months. In fact, the value of resistance R_e of the LATP membrane was determined from the low-frequency intercept with the *x* axis changes less than 10 % in 21 months of storage.

We calculated the LATP membrane's ionic conductivity from the low-frequency intercept R_e in Fig. 3a and the membrane thickness, and this conductivity value is very close to that obtained from the data in Fig. 3b. Therefore, the replacement of one of the gold electrodes with liquid electrolyte did not affect the membrane resistance during 21 months of storage and did not generate new features on the impedance spectra.

The fact that the value of membrane resistance R_e remains practically constant during long-term storage is strong evidence that the LATP membrane is chemically stable to the aqueous electrolyte employed in the cell.

One of the key features of the PLE is that it de-couples the lithium electrode from the air electrode environment allowing complex tailoring of the aqueous electrolyte to enhance Li-Air performance. This is illustrated definitively through the use of aqueous NH_4Cl electrolyte which on Li-Air cell discharge liberates highly hygroscopic LiCl into the air electrode which then scavenges H_2O from ambient air [40–42]. As the Li-Air cell is discharged, a fairly complex reaction[1] takes place which can be viewed in its simplest case as such:

$$2\,Li + 2\,NH_4Cl + {}^1/_2\,O_2 \rightarrow 2\,NH_3\uparrow + H_2O + 2\,LiCl \qquad (1)$$

$$2\,Li + {}^1/_2\,O_2 + H_2O \rightarrow 2\,LiOH \qquad (2)$$

As one can see from the data for aqueous Li-Air cells shown in Fig. 10, the discharge curves exhibit two typical regions: the initial discharge where the voltage decreases linearly and then a long plateau where most of the capacity is delivered. An ammonia gas detector placed in the environmental chamber, where the cells were being discharged, confirmed NH_3 gas evolution during the initial stage of discharge corresponding to the first region on the discharge curves. We performed post-mortem analysis of cells at various stages of discharge and measured the pH of cell electrolyte. We found that during the first stage of discharge, the pH of cell electrolyte rapidly increased from 4.5 to approximately 8.5 and then slowly increased to approximately 9.5, which is in good agreement with reaction (1). Since NH_3 and NH_4Cl dissolved in water form an ammonia buffer solution, the electrolyte pH stabilizes at a value below 10. According to reaction (2), when all NH_4Cl in battery electrolyte is converted to LiCl and NH_3, further discharge should lead to the formation of LiOH and a significant increase in electrolyte pH. Post-mortem analysis of cells at the second stage of discharge corresponding to the plateau region on the discharge curve indicated the presence of a solid discharge product and an increase in pH to a value greater than 13. These findings are in good agreement with reaction (2). For our cells, the major fraction (80–85 %) of discharge capacity was delivered in the two-phase (solid–liquid) region, corresponding to the long plateau on the discharge curves.

Since the first stage of discharge involves conversion of NH_4Cl to hygroscopic LiCl, the initial amount of water loaded into the cell prior to discharge can be significantly less than the amount of water required for a full discharge. The process of bringing water into the cathode is also affected by the presence of other species in solution. The rate at which water is scavenged from the external atmosphere is determined by a number of variables including depth of discharge, distribution and morphology of the LiOH and LiCl hydrates (and/or complexes formed on cell discharge), structure and composition of the porous air electrode, and the water permeability of the gas diffusion membrane. All of these factors must be

[1] It is likely that a distribution of LiOH and LiCl hydrates and/or complexes is formed on cell discharge; the presence of the intermediate Li_2O_2 solid product is also possible.

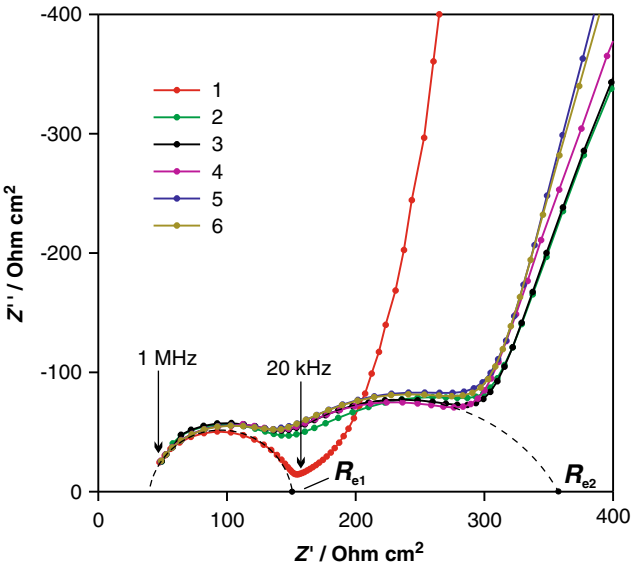

Fig. 11 Impedance spectra for LATP membrane exposed to 2.0 M citric acid electrolyte. Membrane thickness is 160 μm. Length of exposure: *1*—less than 1 day, *2*—4 days, *3*—10 days, *4*—13 days, *5*—20 days, *6*—21 days. *Arrows* indicate characteristic frequencies

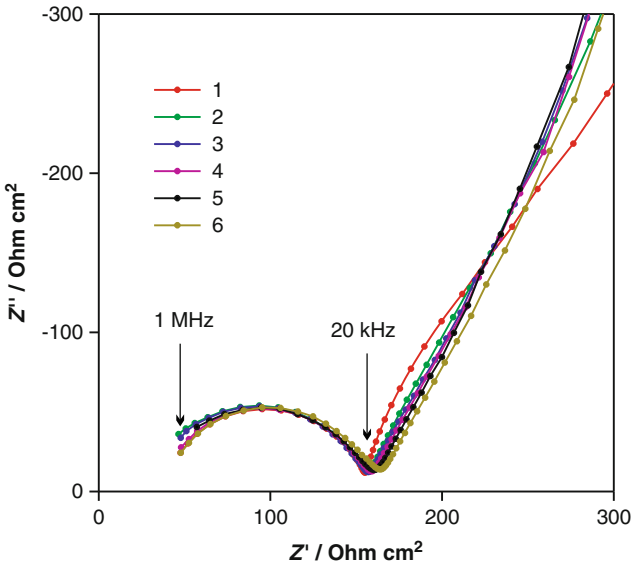

Fig. 13 Beneficial effect of imidazole on the impedance behavior of LATP exposed to citric acid. Membrane thickness is 150 μm. Length of exposure: *1*—less than 1 day, *2*—4 days, *3*—5 days, *4*—6 days, *5*—11 days, *6*—13 days. *Arrows* indicate characteristic frequencies

considered when designing an air electrode for particular applications, since the Li-Air cell behavior (power and capacity) will be affected by the external environment.

Rechargeable aqueous Li-Air Although we have demonstrated superb specific energy for primary Li-Air cells using aqueous NH_4Cl/LiCl electrolytes, these electrolytes are not appropriate for secondary cells (partly due to the formation of NH_3 during discharge). We have explored a number of polyprotic acids for use in secondary Li-Air cells. The use of polyprotic acid delays generation of insoluble discharge products and allows rejection of CO_2 at high states of cell charge. In general, strong inorganic acids are poor choices since they attack the LATP membranes and in some cases the corresponding salts are practically insoluble in water (e.g., Li_3PO_4) leading to rapid precipitation on discharge and/or limited reversibility. Accordingly, PolyPlus uses polyprotic organic acids in its rechargeable Li-Air cells [43]. Two such electrolytes are based on citric and malonic acids.

The Li-Air cell reactions for malonic and citric acid electrolytes are shown below.

Malonic acid

Anode:

$$Li \rightarrow Li^+ + e^-$$

Cathode:

$$4\,H_2C_3H_2O_4 + O_2 + 4\,e^- \rightarrow 4\,HC_3H_2O_4^- + 2\,H_2O \quad (1)$$

$$4\,HC_3H_2O_4^- + O_2 + 4\,e^- \rightarrow 4\,C_3H_2O_4^{2-} + 2\,H_2O \quad (2)$$

Citric acid

Anode:

$$Li \rightarrow Li^+ + e^-$$

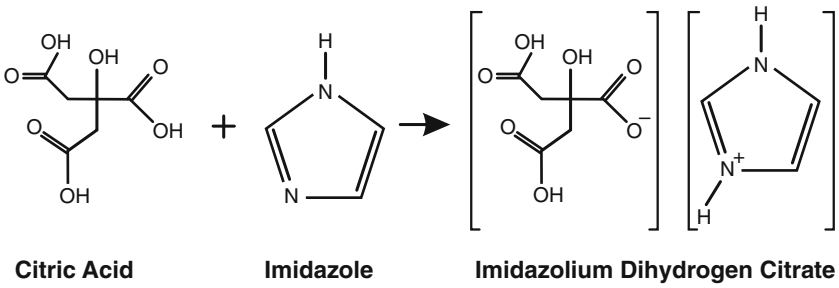

Fig. 12 Acid–base reaction of citric acid and imidazole

Cathode:

$$4\ H_3C_6H_5O_7 + O_2 + 4\ e^- \rightarrow 4\ H_2C_6H_5O_7^- + 2\ H_2O \quad (1)$$

$$4\ H_2C_6H_5O_7^- + O_2 + 4\ e^- \rightarrow 4\ HC_6H_5O_7^{2-} + 2\ H_2O \quad (2)$$

$$4\ HC_6H_5O_7^{2-} + O_2 + 4\ e^- \rightarrow 4\ C_6H_5O_7^{3-} + 2\ H_2O \quad (3)$$

The nature of the polyprotic organic acid has a large impact on the stability of the solid electrolyte membrane; for the case of the electrolyte based on diprotic malonic acid, we did not observe impedance rise for the exposed LATP membrane. However, for some polyprotic organic acids including citric acid, LATP membranes do show evidence of degradation on storage manifesting itself as formation of resistive layers on the membrane surface. Stability of LATP solid electrolyte membranes in citric acid is shown in Fig. 11. We observed a rise in the active resistance of the membrane from its initial value of R_{e1} (153 Ohm cm^2) to a significantly higher value of R_{e2}, which stabilized at over 360 Ohm cm^2 after several days of storage. This instability can be addressed by neutralization of the most acidic proton in the polyprotic organic acid with lithium hydroxide. The downside of this approach is the forfeiture of one of the active protons leading to lower cell capacity and formation of solid product earlier during discharge. We found a novel way to adjust pH without loss of active protons by introduction of imidazole. The reaction of citric acid with imidazole is shown in Fig. 12.

A dramatic improvement in LATP stability was observed for the case where imidazole was added to the citric acid electrolyte (Fig. 13); even after 13 days of immersion, the shape of the impedance plot was almost identical to that observed for a pristine sample. We also determined the anodic stability of imidazole in the potential range selected for Li-Air cell cycling as shown in Fig. 14; the large anodic current observed for the buffer solution corresponds to the oxygen evolution reaction. In Fig. 14, one can see that the anodic process is shifted in the positive direction and no additional electrochemical features are observed, indicating good anodic stability for the imidazole electrolyte.

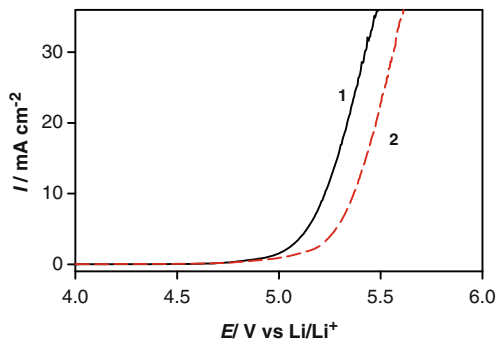

Fig. 14 Anodic stability of imidazole determined by cyclic voltammetry (scan rate of 0.5 mV/s) on glassy carbon electrode in electrolytes containing imidazole and phosphate buffer. *1*—buffer solution, 0.71 M Na_2HPO_4 and 0.1 M H_3PO_4, pH = 7; *2*—0.5 M imidazole, 0.6 M Na_2HPO_4, and 0.26 M H_3PO_4, pH = 7

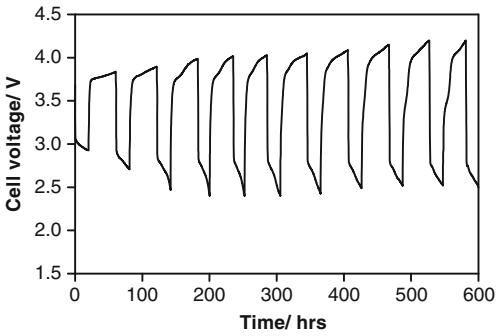

Fig. 15 Cycling performance of aqueous Li-Air cells having an electrolyte based on 2.0 M imidazolium dihydrogen citrate. Discharge rate was 0.5 mA/cm^2. Charge rate was 0.25 mA/cm^2. All discharges lasted 20 h or were limited by a cutoff voltage of 2.4 V. All charge capacities were equal to the capacities of the discharges immediately preceding them or were limited by a cutoff voltage of 4.2 V

We then built aqueous Li-Air cells using imidazolium dihydrogen citrate electrolyte in the air cathode. As is shown in Fig. 15, we observed about ten cycles at a current density of 1 mA/cm^2 and an areal capacity of 5 mAh/cm^2 (C/5) before the air electrode began to polarize. However, we observed

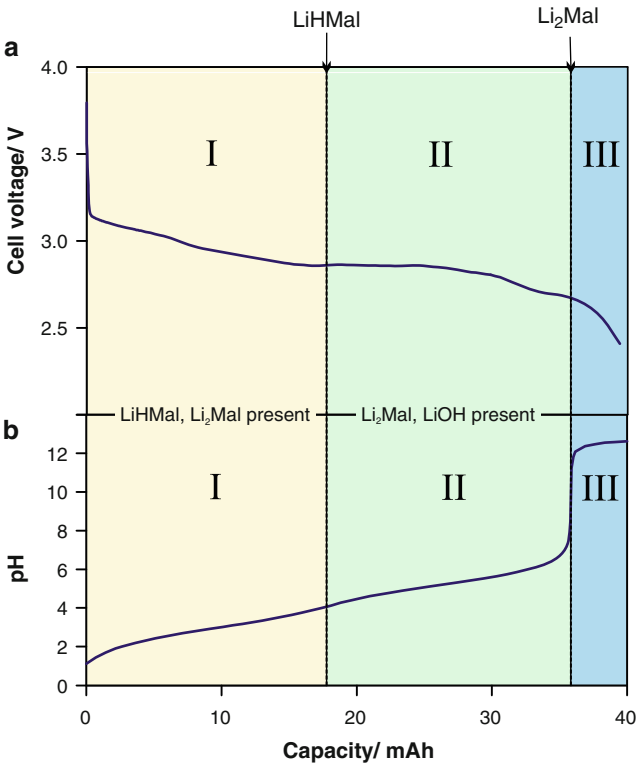

Fig. 16 **a** Discharge voltage profile of aqueous Li-Air cell having an electrolyte based on 4.0 M malonic acid. **b** Experimental titration curve for the same electrolyte plotted as a function of cell discharge capacity

much better cycling behavior for Li-Air cells built with air electrodes having malonic acid electrolyte.

A discharge curve for a Li-Air cell having malonic acid electrolyte is shown in Fig. 16 overlaid with the experimental titration curve for the cell electrolyte re-plotted as a function of capacity (mAh). As can be seen from the data, the pH of the air electrode varies from about 1 for a fully charged cell to more than 12 for a fully discharged air electrode. As one can see, there are three distinct regions in the pH curves corresponding to the titration of two active protons, leading finally to a region of high pH. Importantly, using such polyprotic acid-based aqueous electrolytes, we have demonstrated extended cycling for aqueous Li-Air cells. In Fig. 17, we show the cycling behavior for Li-Air cells having malonic acid electrolytes.

For the case of malonic acid, Li-Air cells delivered more than 75 cycles at 5 mAh/cm^2 capacity, at discharge current densities of 1 mA/cm^2 (C/5), and at charge rates of 0.5 mA/cm^2, for a total cycled capacity of 375 mAh/cm^2 (75 cycles of 5 mAh/cm^2 each). To the best of our knowledge, this is the largest cycled capacity ever reported for Li-Air chemistry. Aqueous Li-Air cells having malonic acid electrolyte also demonstrate reasonably good high current pulse behavior as can be seen from Fig. 18. We believe that the present limitation to cycling of aqueous rechargeable Li-Air might be mediated through better management of the water balance between the air electrode and the external environment.

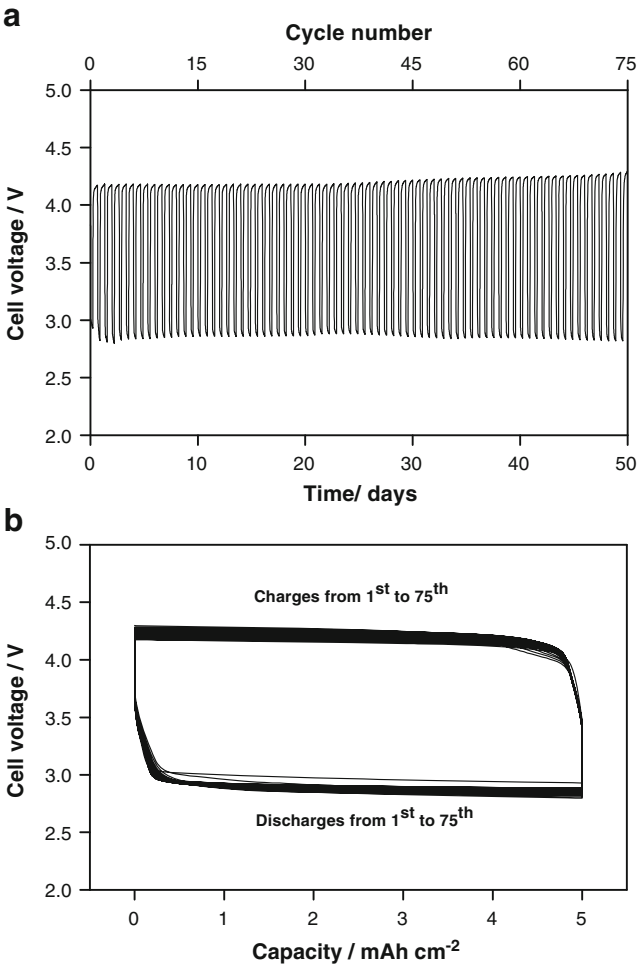

Fig. 17 Cycling behavior of aqueous Li-Air cell having 4.0 M malonic acid electrolyte **a** as a function of time and **b** as a function of capacity. The cell was discharged at a rate of 1.0 mA/cm^2 for 5 h and charged at 0.5 mA/cm^2 for 10 h

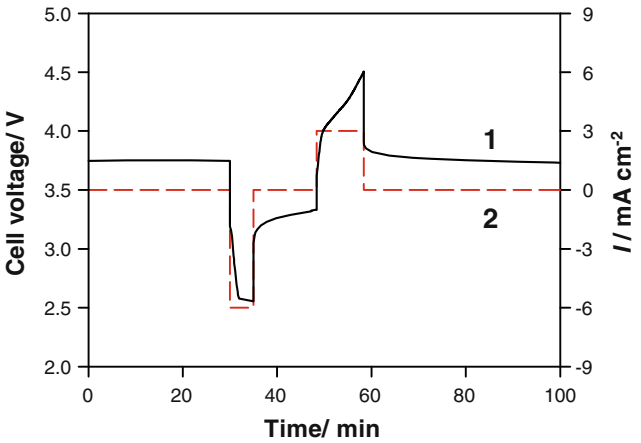

Fig. 18 High-rate pulse behavior of rechargeable aqueous Li-Air cell having 4.0 M malonic acid electrolyte. The cell was discharged at a rate of 6.0 mA/cm^2 for 5 min and charged at 3.0 mA/cm^2 for 10 min. *1*—cell voltage, *2*—current density

Conclusions

Lithium-air chemistry offers the potential for unprecedented energy density and a step change relative to existing commercial batteries. In our opinion, the use of a PLE is a basic requirement for both nonaqueous and aqueous Li-Air technologies. In all cases, the use of a PLE leads to a self-discharge rate of effectively zero. For aqueous Li-Air, the need for a PLE is obvious. However, even for nonaqueous Li-Air, it appears that the use of a PLE could be necessary to enable the use of electrolytes stable to lithium peroxide and superoxide but not lithium metal and to protect the negative electrode from reaction with moisture in ambient air. Nonaqueous Li-Air chemistry is clearly plagued by a number of complex technical hurdles as discussed above. The situation with rechargeable aqueous Li-Air cells is much better. We have demonstrated good cycling at reasonable current densities (C/5 discharge) and high current densities for short bursts (>C rate for 5 min). We have also demonstrated that primary aqueous Li-Air batteries can achieve spectacular specific energies of over 800 Wh/kg.

Acknowledgments This work was funded in part by the ARPA-E of the U.S. Department of Energy and by the U.S. Army CERDEC. The authors also acknowledge the participation of V. Loginova in the experimental work and helpful discussions with Dr. P.N. Ross of the Lawrence Berkeley National Laboratory in Berkeley, CA.

References

1. Visco SJ, Nimon E, De Jonghe LC (2009) In: Garche J (ed) Encyclopedia of electrochemical power sources. Elsevier, Amsterdam 4:376
2. Nimon YS, Visco SJ (2010) US Patent 7645543, filed Feb 3, 2004
3. Visco SJ, Katz BD, Nimon YS (2007) US Patent 7282295, filed Apr 14, 2004
4. Visco SJ, Nimon YS, Katz BD (2007) US Patent 7282296, filed Oct 14, 2003
5. Visco SJ, Nimon YS, Katz BD, Petrov A (2010) US Patent 7824806, filed Aug 8, 2006
6. Bruce PG, Freunberger SA, Hardwick LJ, Tarascon JM (2012) Nat Mat 11:19
7. Christiansen J, Albertus P, Sanchez-Carrera RS, Lohmann T, Kozinsky B, Leidtke R, Ahmed J, Kojic A (2012) J Electrochem Soc 159:R1–R30
8. Peng Z, Freunberger SA, Chen Y, Bruce PG (2012) Science 337: 563–566
9. Walker W, Giordani V, Uddin J, Bryantsev VS, Chase GV, Addison D (2013) J Am Chem Soc 135:2076–2079
10. Visco SJ, Nimon E, Katz BD, De Jonghe LC, Chu MY (2004) In: Abstr Int Meet Lithium Batt. Nara, Japan, 53
11. Visco SJ, Nimon E, Katz BD, De Jonghe LC, Chu MY (2004) In: Abstr Int Meet Lithium Batt. Nara, Japan 396
12. Visco SJ, Nimon E (2004) In: Abstr Int Meet Lithium Batt. Nara, Japan 397
13. Goodenough JB, Hong HYP, Kafalas JA (1976) Mater Res Bull 11: 203–220
14. Abraham KM, Jiang Z (1996) J Electrochem Soc 143:1–5
15. Aurbach D, Daroux M, Faguy P, Yeager E (1991) J Electroanal Chem 297:225–244
16. Mizuno F, Nakanishi S, Kotani Y, Yokoishi S, Iba H (2010) Electrochemistry 78:403–405
17. Freunberger SA, Peng Z, Hardwick LJ, Chen Y, Barde F, Bruce PG (2010) In: Proc 218th Electrochem Soc Meet, Las Vegas, Nevada
18. McCloskey BD, Bethune DS, Shelby RM, Girishkumar G, Luntz AC (2011) J Phys Chem Lett 2:1161–1166
19. Visco SJ, Nimon YS (2007) US Patent Application 20070117007, filed Nov 22, 2006
20. Dresser KJ, Prince RN (1969) NASA Contractor report In: Thermophys. Conf. Am. Inst. Aeronaut. San-Francisco, USA
21. Maricle DL, Hodgson WG (1965) Anal Chem 37:1562–1565
22. Peover ME, White BS (1966) Electrochim Acta 11:1061–1067
23. Jain PS, Lal S (1982) Electrochim Acta 27:759–763
24. Bryantsev VS, Uddin J, Giordani V, Walker W, Addison D, Chase GV (2013) J Electrochem Soc 160:A160–A171
25. Xie B, Lee HS, Li H, Yang XQ, McBreen J, Chen LQ (2008) Electrochem Commun 10:1195–1197
26. Li LF, Xie B, Lee HS, Li H, Yang XQ, McBreen J, Huang XJ (2009) J Power Sources 189:539–542
27. Shanmukaraj D, Grugeon S, Gachot G, Laruelle S, Mathiron D, Tarascon JM, Armand M (2010) J Am Chem Soc 132: 3055–3062
28. Mitchell RR, Gallant BM, Shao-Horn Y, Thompson CV (2013) J Phys Chem Lett 4:1060–1064
29. Lee JH, Black R, Popov G, Pomerantseva E, Nan F, Botton G, Nazar LF (2012) Energy Environ Sci 5:9558–9565
30. Lu YC, Gallant BM, Kwabi DG, Harding JR, Mitchell RR, Whittingham MS, Shao-Horn Y (2013) Energy Environ Sci 6:750–768
31. Nimon VY, Visco SJ, De Jonghe LC, Volfkovich YM, Bograchev DA (2013) ECS Electrochem Lett 2:A33–A35
32. McCloskey BD, Speidel A, Scheffler R, Miller DC, Viswanathan V, Hummelshøj JS, Nørskov JK, Luntz AC (2012) J Phys Chem Lett 3: 997–1001
33. Watanabe Y, Kinoshita S, Wada S, Hoshino K, Morimoto H, Tobishima S (2008) J Power Sources 179:770–779
34. Jung HG, Hassoun J, Park JB, Sun YK, Scrosati B (2012) Nat Chem 4:579–585
35. Fu J (1997) Solid State Ionics 96:195–200
36. Fu J (1997) J Am Ceram Soc 80:1901–1903
37. Birke P, Salam F, Döring S, Weppner W (1999) Solid State Ionics 118:149–157
38. West WC, Whitacre JF, Lim JR (2004) J Power Sources 126: 134–138
39. Puech L, Cantau C, Vinatier P, Toussaint G, Stevens P (2012) J Power Sources 214:330–336
40. Visco SJ, De Jonghe LC, Nimon YS, Petrov A, Pridatko K (2012) US Patent 8323820, filed Jun 12, 2009
41. Visco SJ, De Jonghe LC, Nimon YS, Petrov A, Pridatko K (2013) US Patent 8455131, filed Jun 12, 2009
42. Visco SJ, De Jonghe LC, Nimon YS, Petrov A, Pridatko K (2013) US Patent 8389147, filed Jun 12, 2009
43. Visco SJ, Nimon YS, De Jonghe LC, Petrov A, Goncharenko N (2013) US Patent Application 20130045428, filed Aug 17, 2012